

## Spatial Evolution of Water Surface Waves: Numerical Simulation and Experiment of Bichromatic Waves

*Karsten Trulsen*  
SINTEF Applied Mathematics  
Oslo, Norway

*Carl Trygve Stansberg*  
Marintek  
Trondheim, Norway

### ABSTRACT

The modified nonlinear Schrödinger (MNLS) equation for spatial evolution of weakly nonlinear water surface waves is shown to yield good comparisons with experimental measurements of bichromatic waves in a long tank. While linear theory does not predict neither the phase velocity nor the evolution of the envelope well, the cubic nonlinear Schrödinger (NLS) equation improves the prediction of the phase velocity but not the modulation of the envelope. The MNLS equation predicts both the evolution of individual wave crests and the modulation of the envelope over longer fetch, and thus permits accurate forecasting of individual ocean wave crests over a fetch of several tens of wavelengths.

**KEY WORDS:** wave groups, bichromatic waves, nonlinear Schrödinger equation

### INTRODUCTION

Wave grouping is a prominent feature of ocean waves, frequently discussed in the literature. It may be partly responsible for the generation of freak waves. The simplest realization of wave groups is the bichromatic wave, achieved by mixing two monochromatic waves. In the present paper we use experiments of bichromatic waves as a benchmark to assess the capability of three different simulation models to describe wave group evolution. The three models are the linear wave equation, the cubic nonlinear Schrödinger (NLS) equation and the modified nonlinear Schrödinger (MNLS) equation.

It is common to stress the importance of time-domain simulation, as opposed to frequency-domain simulation, of nonlinear ocean waves. However, conventional methods for measuring waves in the laboratory and the field yield time series at selected spatial locations. Space evolution is implied between the selected points. For such cases a time-domain simulator is likely not very useful, or at best quite difficult to initialize. A better approach is to interchange the role of space and time in the evolution equation to obtain a genuine space-domain simulator. The nonlinear

Schrödinger equation and its higher order modifications are particularly well-suited for this purpose. Lo & Mei (1985) first presented comparisons between experiments and the space evolution predicted by the MNLS equation, and obtained good results.

Recently the MNLS equation was enhanced with exact linear dispersion (Trulsen et al. 2000) for better bandwidth resolution for application to realistic ocean wave spectra. This approach is based on the assumption that the spectrum to leading order of approximation is narrow-banded. The remaining part of the spectrum is reconstructed only to the extent that it is nonlinearly forced by, and thus coherent with, the linear waves near the spectral peak. Special care must be taken for proper initialization to distinguish between linear free waves and nonlinearly forced waves. To this end we have developed an iterative technique by which the extracted spectrum of linear free waves is refined until exact reconstruction of the measured complex spectrum has been achieved within the bandpass region.

The natural spatial scale of nonlinear modulation is  $\eta = \epsilon^2 k_c x$ , where  $\epsilon = k_c a_c$  is the wave steepness,  $k_c$  and  $a_c$  are characteristic scales for wavenumber and amplitude, and  $x$  is the fetch. The present simulation results of the MNLS equation suggest that prediction of the evolution of individual wave crests is good at least up to  $\eta = 3$ , while it becomes poor for  $\eta > 5$ . If we assume  $\epsilon = 0.1$  for typical ocean waves, then  $\eta = 5$  roughly corresponds to 80 wavelengths. For 12 s waves on deep water, corresponding to 220 m wavelength, that could imply up to half an hour warning for individual wave crests for propagation over 16 km in long-crested seas. Proper verification should be done against experimental data for short-crested seas.

Similar work with the cubic nonlinear Schrödinger (NLS) equation was done by Shemer et al. (1998) for deep water and with the Korteweg de-Vries equation for shallow water by Kit et al. (2000). The Zakharov equation, which in its original form is a time-domain equation, has been discretized for application to measurements (Rasmussen & Stiassnie 1999); recently it was cast as a space domain simulator for one horizontal dimension by She-

## THE EXPERIMENT

The experiments were carried out in the 260 m long and 10.5 m wide towing tank at Marintek. Waves were generated by a horizontally double-hinged flap-type wave maker. The depth of the tank is 10 m for the first 80 m closest to the wave maker, and 5 m elsewhere. A vertical bottom jump connects the two tank parts. A sloping beach is located at the far end of the tank opposite the wave maker. The wave elevation was measured by wave staffs at different locations simultaneously downstream the tank, see figure 1.

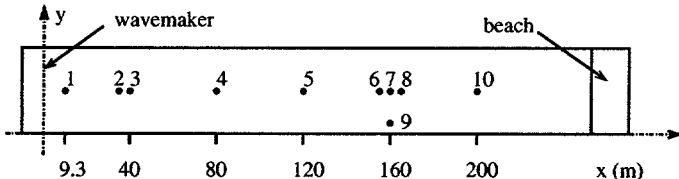


Figure 1: Sketch of the wave tank with the locations of the wave staffs.

The time series measured by probe 1 at 9.3 m is used in this paper for initialization of the numerical simulations. Probe 2 is at 40 m and is 0.5 m in front of probe 3. Probes 6 and 8 are 0.4 m ahead of and behind probe 7 at 160 m. Probe 9 is 1.5 m from the tank wall and serves to assess the importance of transversal modulations.

We consider two experiments with bichromatic waves (test 60 and test 61) which were done according to the following specifications:

Test	Wave periods		Wave heights	
	$T_1$ [s]	$T_2$ [s]	$H_1$ [m]	$H_2$ [m]
60	1.90	2.10	0.16	0.16
61	0.95	1.05	0.04	0.04

Further details of the experiment have been reported in Stansberg (1993, 1995, 1998).

## MATHEMATICAL MODEL FOR SPACE-DOMAIN SIMULATION

Starting from the inviscid equations for potential flow, normalized by the characteristic wavenumber  $k_c$  and frequency  $\omega_c$ , and assuming constant depth  $h$  which is great in comparison with the wavelength  $k_c h \gg 1$ , we make an assumption that the velocity potential  $\phi$  and surface displacement  $\zeta$  of the wave field can be expanded in harmonic expansions

$$\phi = \bar{\phi} + \frac{1}{2} \left( A e^{i(x-t)+z} + A_2 e^{2i(x-t)+2z} + A_3 e^{3i(x-t)+3z} + \dots + \text{c.c.} \right), \quad (1)$$

$$\zeta = \bar{\zeta} + \frac{1}{2} \left( B e^{i(x-t)} + B_2 e^{2i(x-t)} + B_3 e^{3i(x-t)} + \dots + \text{c.c.} \right). \quad (2)$$

Here  $(x, y)$  and  $z$  are horizontal and vertical coordinates,  $t$  is time,  $\bar{\phi}$  and  $\bar{\zeta}$  are mean field variables, and  $A, A_n, B, B_n$  are complex harmonic amplitudes. The complex conjugate is denoted by "c.c."

Recently, Trulsen et al. (2000) explained how the MNLS equation can be enhanced with exact linear dispersion by introducing a pseudo-differential operator for the linear part. In two horizontal dimensions it reads

$$\frac{\partial B}{\partial t} + L(\partial_x, \partial_y)B + \frac{i}{2}|B|^2 B + \frac{3}{2}|B|^2 \frac{\partial B}{\partial x} + \frac{1}{4}B^2 \frac{\partial B^*}{\partial x} + i \frac{\partial \bar{\phi}}{\partial x} B = 0 \quad \text{at } z = 0, \quad (3)$$

$$\frac{\partial \bar{\phi}}{\partial z} = \frac{1}{2} \frac{\partial}{\partial x} |B|^2 \quad \text{at } z = 0, \quad (4)$$

$$\nabla^2 \bar{\phi} = 0 \quad \text{for } -h < z < 0, \quad (5)$$

$$\frac{\partial \bar{\phi}}{\partial z} = 0 \quad \text{at } z = -h, \quad (6)$$

where the pseudo-differential operator  $L$  is

$$L(\partial_x, \partial_y) = i \left\{ [(1 - i\partial_x)^2 - \partial_y^2]^{1/4} - 1 \right\}. \quad (7)$$

These equations can be inverted with respect to space and time to yield a space-domain formulation

$$\frac{\partial B}{\partial x} + \mathcal{L}(\partial_t, \partial_y)B + i|B|^2 B - 8|B|^2 \frac{\partial B}{\partial t} - 2B^2 \frac{\partial B^*}{\partial t} - 4i \frac{\partial \bar{\phi}}{\partial t} B = 0 \quad \text{at } z = 0, \quad (8)$$

$$\frac{\partial \bar{\phi}}{\partial z} = -\frac{\partial}{\partial t} |B|^2 \quad \text{at } z = 0, \quad (9)$$

$$\nabla^2 \bar{\phi} = 0 \quad \text{for } -h < z < 0, \quad (10)$$

$$\frac{\partial \bar{\phi}}{\partial z} = 0 \quad \text{at } z = -h. \quad (11)$$

Here we have used the fact that  $\partial \bar{\phi} / \partial x = -2\partial \bar{\phi} / \partial t$  to the leading order. This transformation should also be reflected in the Laplacian of the induced velocity potential in (10). The pseudo-differential operator becomes

$$\mathcal{L}(\partial_t, \partial_y) = -i \left\{ [(1 + i\partial_t)^4 + \partial_y^2]^{1/2} - 1 \right\}. \quad (12)$$

By expanding the linear pseudo-differential operators  $L$  or  $\mathcal{L}$  in power series expansions and truncating at appropriate orders, we recover the MNLS equation of Dysthe (1979) and the broader bandwidth equation of Trulsen & Dysthe (1996). Furthermore by truncating the nonlinear part to retain only the leading cubic nonlinear term, we recover the standard cubic nonlinear Schrödinger equation.

We remark that in one horizontal dimension ( $x$ ), the operator  $\mathcal{L}$  is algebraic. In this paper we consider the one-dimensional ( $x$ ) limit of (8)–(12). The MNLS equation becomes

$$\frac{\partial B}{\partial x} + 2 \frac{\partial B}{\partial t} + i \frac{\partial^2 B}{\partial t^2} + i|B|^2 B - 8|B|^2 \frac{\partial B}{\partial t} - 2B^2 \frac{\partial B^*}{\partial t} - 4i \frac{\partial \bar{\phi}}{\partial t} B = 0 \quad \text{at } z = 0. \quad (13)$$

The cubic nonlinear (NLS) equation is

$$\frac{\partial B}{\partial x} + 2\frac{\partial B}{\partial t} + i\frac{\partial^2 B}{\partial t^2} + i|B|^2 B = 0. \quad (14)$$

The linear equation is

$$\frac{\partial B}{\partial x} + 2\frac{\partial B}{\partial t} + i\frac{\partial^2 B}{\partial t^2} = 0. \quad (15)$$

The reconstruction of the surface displacement (2) is achieved by the formulas

$$\bar{\zeta} = -\frac{\partial \bar{\phi}}{\partial t}, \quad (16)$$

$$B_2 = \frac{1}{2}B^2 + iB\frac{\partial B}{\partial t}, \quad (17)$$

and

$$B_3 = \frac{3}{8}B^3. \quad (18)$$

## NUMERICAL IMPLEMENTATION

The present implementation is based on imposing periodic boundary conditions in time, which is appropriate for the experimental data under consideration. Letting  $B$  be represented by a suitable number of modes  $M$ , the Fourier transform pair for  $B$  is defined by

$$\begin{aligned} \hat{B}(x, \omega_j) &= \frac{1}{M} \sum_{m=0}^{M-1} B(x, t_m) e^{i\omega_j t_m}, \\ B(x, t_m) &= \sum_{-\frac{M}{2} < j \leq \frac{M}{2}} \hat{B}(x, \omega_j) e^{-i\omega_j t_m}, \end{aligned} \quad (19)$$

where  $\omega_j = 2\pi j/T$ ,  $t_m = mT/M$ , and  $T$  is the length of the periodic domain.

The numerical implementation has been documented elsewhere (Lo & Mei 1985; Trulsen & Dysthe 1997). The differential equation is solved by an operator splitting method. The nonlinear part is integrated by a finite difference method in physical space, while the linear dispersive part is solved exactly in Fourier space. In particular, we remark that the full pseudo-differential operator becomes algebraic in Fourier space, and thus integration of the exact linear dispersive part in two horizontal dimensions can be done as fast and easily as for any of the truncated equations.

## INITIALIZATION

The surface displacement  $\zeta(x, t)$  is measured at a fixed position  $x$  with a sampling period  $\tau$ , providing a time series  $\zeta(x, t_n)$  for  $t_n = n\tau$ ,  $n = 0, 1, 2, \dots, N-1$  over a total time interval  $T = N\tau$ . The Fourier transform pair for the surface displacement is

$$\begin{aligned} \hat{\zeta}(x, \omega_j) &= \frac{1}{N} \sum_{n=0}^{N-1} \zeta(x, t_n) e^{i\omega_j t_n}, \\ \zeta(x, t_n) &= \sum_{-\frac{N}{2} < j \leq \frac{N}{2}} \hat{\zeta}(x, \omega_j) e^{-i\omega_j t_n}, \end{aligned} \quad (20)$$

where  $\omega_j = 2\pi j/T$ .

It is in general not possible to deduce what portion of the power spectrum is due to free or bound waves based on a time series from a single point. A good approximation is to construct  $\hat{B}$  by bandpassing the complex spectrum  $\hat{\zeta}$  around a central frequency. To this end we determine the characteristic frequency  $\omega_c$  from the mean of the dimensional frequency power spectrum

$$\omega_c = \frac{2\pi M_0}{T} \approx \frac{\sum_j |\omega_j| |\hat{\zeta}_j|^2}{\sum_j |\hat{\zeta}_j|^2}, \quad (21)$$

such that  $M_0$  is an integral number of central wave oscillations in the computational domain. The corresponding characteristic wavenumber  $k_c$  is computed from the linear dispersion relation.

The complex spectrum of the first harmonic  $\hat{B}$  is first assigned by bandpassing  $M_{bp}$  components of the desired complex spectrum  $\hat{\zeta}_j$  centered around  $\omega_c$ ,

$$\hat{B}(x, \omega_j) = 2c_j e^{-ix} \hat{\zeta}(x, \omega_j + M_0) \quad \text{for } |j| \leq \frac{M_{bp}}{2}, \quad (22)$$

where  $c_j$  are adjustable coefficients initially set to unity. As far as  $\hat{B}$  is concerned,  $\omega_j$  is a modulation frequency relative to the characteristic frequency  $\omega_c$ .

The complex coefficients  $c_j$  are adjusted in an iterative manner to compensate for the higher-order nonlinear modification of the measured wave spectrum (16)–(18). If the desired spectrum is  $\hat{\zeta}_j$ , suppose that after an iteration the reconstruction of the spectrum is  $\tilde{\zeta}_j$  and the reconstruction of the linear first-harmonic part of the spectrum is  $\tilde{\zeta}_{1,j}$ , then the new iterate for  $c_j$  is

$$c_j = 1 - \frac{\tilde{\zeta}_j - \tilde{\zeta}_{1,j}}{\hat{\zeta}_j} \quad (23)$$

The iteration scheme is stopped when the adjustment coefficients have converged, typically after 10–20 iterations.

## COMPARISON BETWEEN SIMULATION AND EXPERIMENT

Experimental test 60 is periodic with period 39.9 s. We use a computational domain of length 279.3 s, corresponding to 7 periods, after skipping the first 19.7 s of startup. The nondimensional depth is  $k_c h = 10$  for the first 80 m and  $k_c h = 5$  for the rest of the tank, however we here present simulations using  $k_c h = 10$  for the entire tank. Simulations with  $k_c h = 5$  revealed only insignificant modifications for large fetch, thus we believe that as far as this comparison between experiment and simulations is concerned, the effect of the jump at 80 m is not important.

The time series measured at wave staff 1 is used for initialization. Here the transient effects of startup do not occur in the computational domain. At successive wave staffs, the transient effects of startup propagate into the computational domain, but are not accounted for in the numerical simulation. We present results from the last period in the computational domain which remains unaffected by transient effects of startup for the duration of the simulation. Measurements and initialization at staff 1 is shown in figure 2.

Linear wave theory at staffs 2, 4 and 5 are shown in figures 3–5. Linear theory underpredicts both the phase and group velocities observed in the experiments. Linear theory also does not account for the change in shape of the wave group.

NLS simulation results at staffs 2, 4 and 5 are shown in figures 6–8. The NLS equation accounts for a nonlinear increase

in phase velocity, and yields good agreement with the observed phase velocity in the experiment. The NLS equation does not account for the nonlinear increase in group velocity. The NLS equation does account for the nonlinear increase in amplitude of the group, but does not capture the asymmetric forward-leaning evolution seen in the experiments.

MNLS simulation results at staffs 2, 4, 5, 7 and 10 are shown in figures 9–13. The MNLS equation accounts for nonlinear increase in both the phase and group velocities, in good agreement with the experimental observations. The nonlinear increase in amplitude of the group and the asymmetric forward-leaning evolution of the group seen in the experiments are also captured.

Experiment 61 was done for shorter wavelength and larger steepness, yielding an effectively much longer tank. The waves are periodic with period 19.95 s. We use a computational domain of length 199.5 s corresponding to 10 periods, after skipping the first 270.5 s of the time series. The nondimensional depth is  $k_c h = 40$  for the first 80 m and  $k_c h = 20$  for the rest of the tank. These depths are effectively infinite as far as experiment 61 is concerned.

The time series measured at wave staff 1 is used for initialization and is shown in figure 14.

MNLS simulation results at staffs 2, 4 and 5 are shown in figures 15–17. In figure 15 we observe that the qualitative features of group splitting are well captured. The last figure 17 reveals that the simulation results of the MNLS equation become unreliable for large fetch.

## CONCLUSION

We have shown that the MNLS equation can be used to predict the evolution of individual long wave crests at least up to the dimensionless scale for evolution  $\eta = \epsilon^2 k_c x = 3$ . The prediction becomes poor for  $\eta > 5$ , and is unreliable for  $\eta > 8$ . If we set  $\epsilon = 0.1$  for typical ocean waves, then  $\eta = 5$  roughly corresponds to 80 wavelengths. For 12 s waves on deep water, corresponding to a wavelength of 220 m, that could imply up to half an hour warning for individual wave crests at a distance of up to 16 km for a long-crested sea.

On the other hand, the NLS equation and the linear theory are not able to predict the evolution well even up to  $\eta = 1$ .

The characteristic qualitative features of bichromatic wave evolution, e.g. nonlinear increase in phase and group velocities, asymmetric forward-leaning evolution of initially symmetric groups, and group splitting, are captured by the MNLS equation. On the other hand, the standard cubic nonlinear Schrödinger (NLS) equation only accounts for the nonlinear increase in the phase velocity. We conclude that the higher order nonlinearities originally found by Dysthe (1979), are essential to explain nonlinear ocean wave evolution, even over short fetch.

These experiments and simulations were done for long-crested waves. It is necessary to perform experiments and simulations for short-crested waves to assess if forecasting of individual wave crests can be done in a realistic short-crested sea. However, for long-crested sea states, we anticipate that this model is capable of accurately forecasting individual wave crests over a fetch of several tens of wavelengths.

## ACKNOWLEDGMENTS

This work has been supported by the Norwegian Research Council through the project “Modeling of extreme ocean waves and ocean wave climate on mesoscale” (139177/431) and by grants from Norsk Hydro and Statoil (ANS025701). The experiment was funded by the Norwegian Research Council.

## REFERENCES

- Dysthe, K. B. (1979). Note on a modification to the nonlinear Schrödinger equation for application to deep water waves. *Proc. R. Soc. Lond. A* **369**, 105–114.
- Kit, E., Shemer, L., Pelinovsky, E., Talipova, T., Eitan, O. & Jiao, H.-Y. (2000). Nonlinear wave group evolution in shallow water. *J. Waterway, Port, Coastal and Ocean Engineering* **126**, 221–228.
- Lo, E. & Mei, C. C. (1985). A numerical study of water-wave modulation based on a higher-order nonlinear Schrödinger equation. *J. Fluid Mech.* **150**, 395–416.
- Rasmussen, J. H. & Stiassnie, M. (1999). Discretization of Zakharov’s equation. *Eur. J. Mech. B/Fluids* **18**, 353–364.
- Shemer, L., Kit, E., Jiao, H.-Y. & Eitan, O. (1998). Experiments on nonlinear wave groups in intermediate water depth. *J. Waterway, Port, Coastal and Ocean Engineering* **124**, 320–327.
- Shemer, L., Jiao, H. Y., Kit, E. & Agnon, Y. (2001). Evolution of a nonlinear wave field along a tank: experiments and numerical simulations based on the spatial Zakharov equation. *J. Fluid Mech.* **427**, 107–129.
- Stansberg, C. T. (1993). *Propagation-dependent spatial variations observed in wavetrains generated in a long wave tank. Data report*. Technical Report MT49 A93–0176, Marintek.
- Stansberg, C. T. (1995). Spatially developing instabilities observed in experimental bichromatic wave trains. In A. J. Grass (Ed.), *26th IAHR Congress (HYDRA 2000)*, volume 3 (pp. 180–185): Thomas Telford.
- Stansberg, C. T. (1998). On the nonlinear behaviour of ocean wave groups. In *Proc. Third International Symposium on Ocean Wave Measurement and Analysis — WAVES’97 (ASCE)*, volume 2 (pp. 1227–1241).
- Trulsen, K. & Dysthe, K. B. (1996). A modified nonlinear Schrödinger equation for broader bandwidth gravity waves on deep water. *Wave Motion* **24**, 281–289.
- Trulsen, K. & Dysthe, K. B. (1997). Frequency downshift in three-dimensional wave trains in a deep basin. *J. Fluid Mech.* **352**, 359–373.
- Trulsen, K., Kliakhandler, I., Dysthe, K. B. & Velarde, M. G. (2000). On weakly nonlinear modulation of waves on deep water. *Phys. Fluids* **12**, 2432–2437.

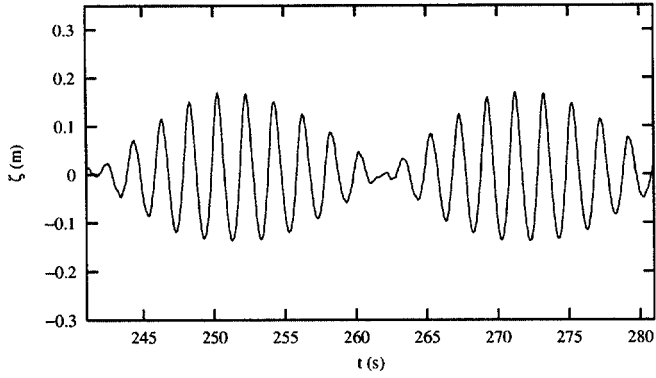


Figure 2: Test 60, wave staff 1 at 9.3 m,  $\eta = 0$ , used for initialization: —, experiment and all wave theories (linear, NLS, MNLS).

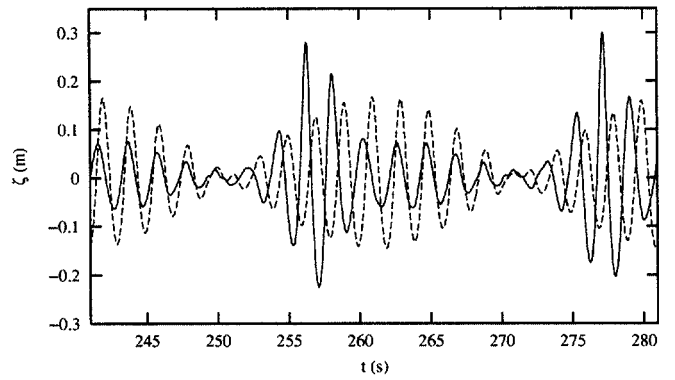


Figure 5: Test 60, staff 5 at 120 m,  $\eta = 1.4$ : —, experiment; --, linear.

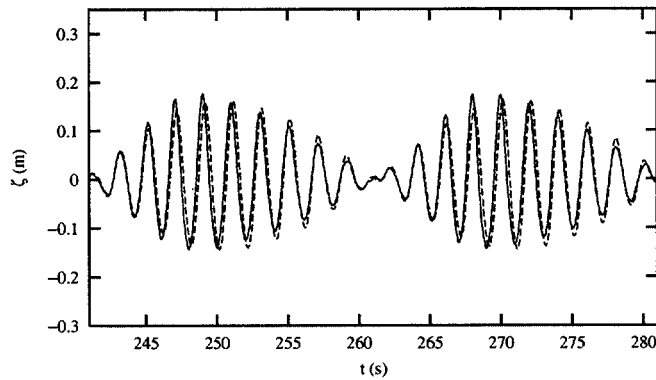


Figure 3: Test 60, staff 2 at 40 m,  $\eta = 0.4$ : —, experiment; --, linear.

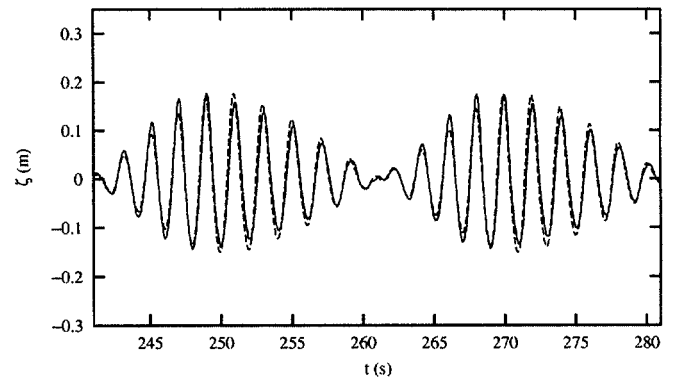


Figure 6: Test 60, staff 2 at 40 m,  $\eta = 0.4$ : —, experiment; --, NLS.

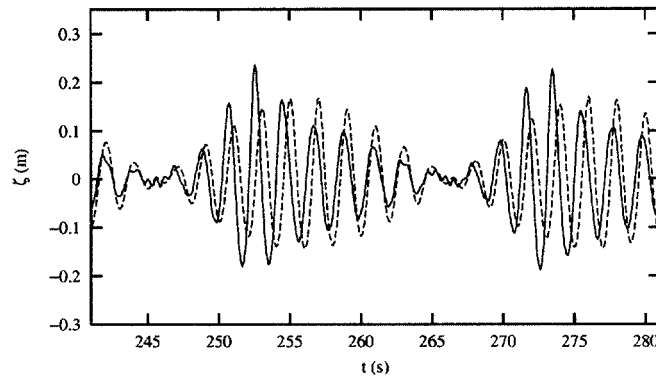


Figure 4: Test 60, staff 4 at 80 m,  $\eta = 0.9$ : —, experiment; --, linear.

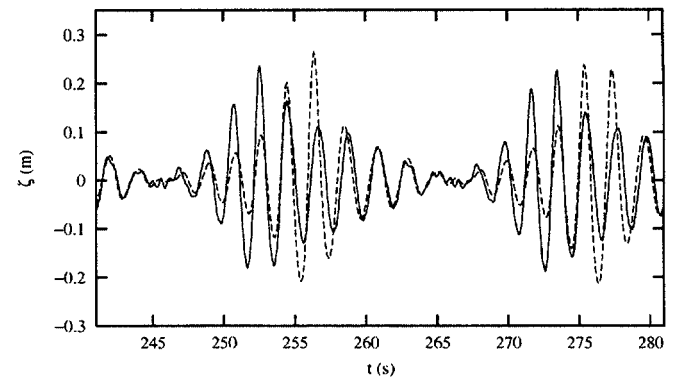


Figure 7: Test 60, staff 4 at 80 m,  $\eta = 0.9$ : —, experiment; --, NLS.

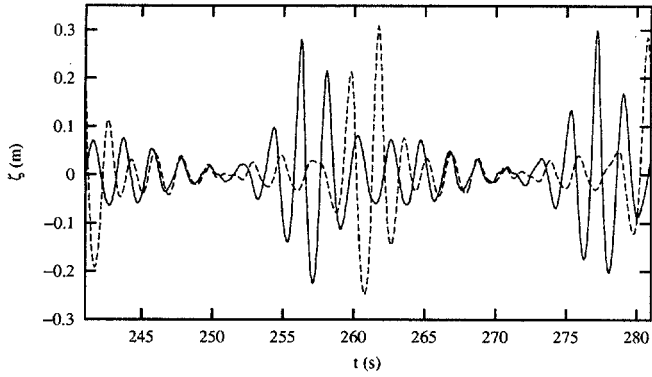


Figure 8: Test 60, staff 5 at 120 m,  $\eta = 1.4$ : —, experiment; --, NLS.

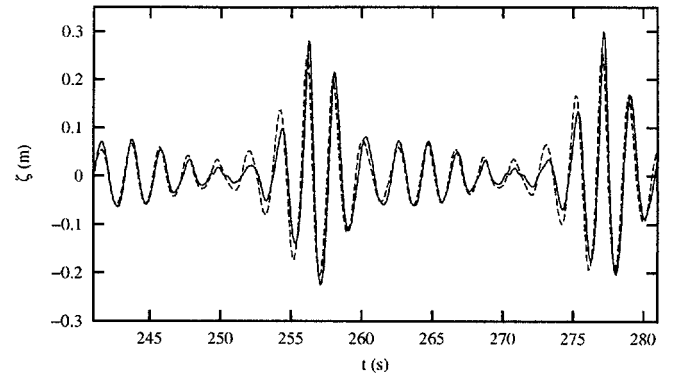


Figure 11: Test 60, staff 5 at 120 m,  $\eta = 1.4$ : —, experiment; --, MNLS.

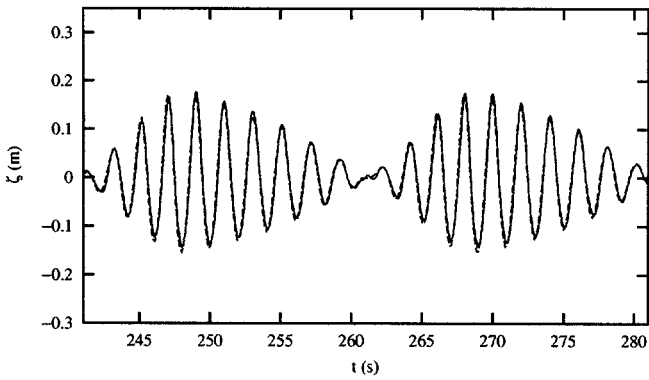


Figure 9: Test 60, staff 2 at 40 m,  $\eta = 0.4$ : —, experiment; --, MNLS.

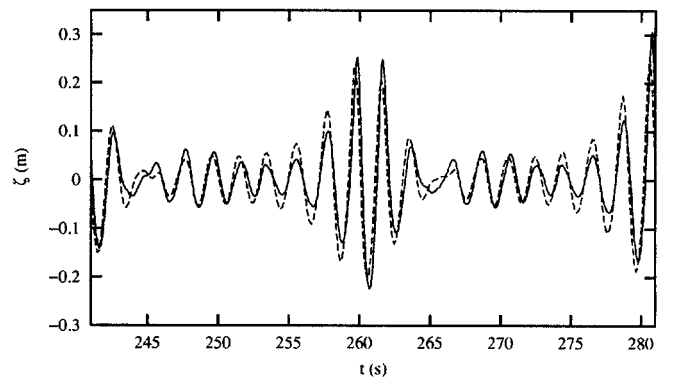


Figure 12: Test 60, staff 7 at 160 m,  $\eta = 1.9$ : —, experiment; --, MNLS.

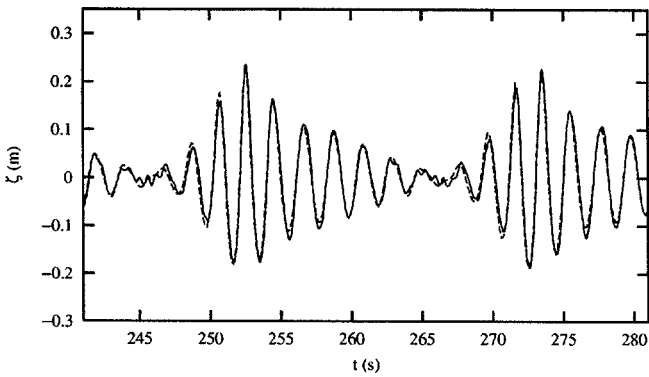


Figure 10: Test 60, staff 4 at 80 m,  $\eta = 0.9$ : —, experiment; --, MNLS.

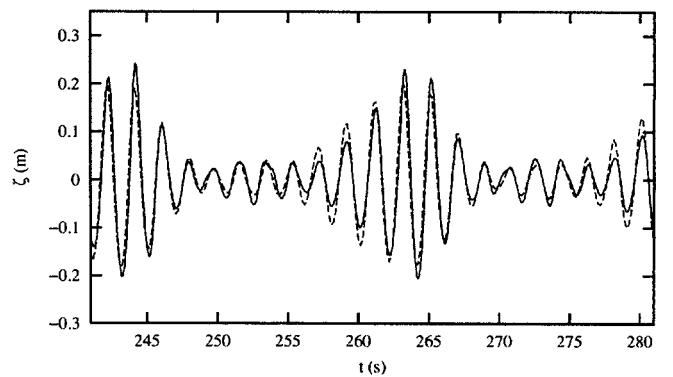


Figure 13: Test 60, staff 10 at 200 m,  $\eta = 2.4$ : —, experiment; --, MNLS.

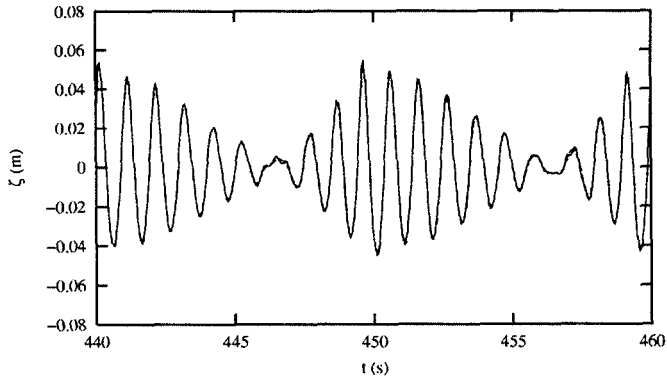


Figure 14: Test 61, staff 1 at 9.3 m,  $\eta = 0$ , used for initialization: —, experiment; - -, MNLS.

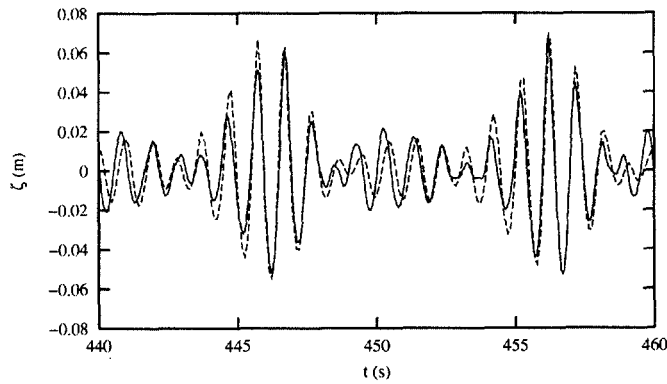


Figure 15: Test 61, staff 2 at 40 m,  $\eta = 2.5$ : —, experiment; - -, MNLS.

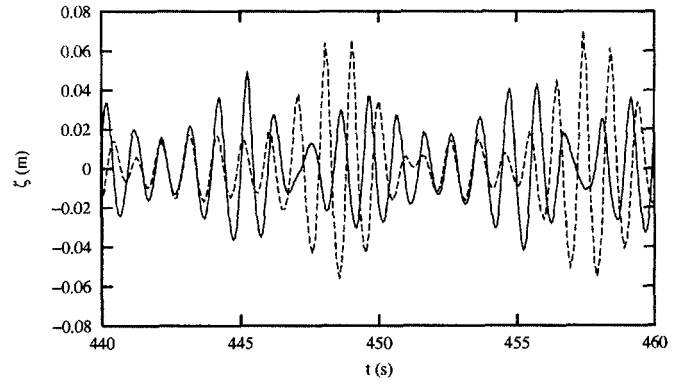


Figure 17: Test 61, staff 5 at 120 m,  $\eta = 8.9$ : —, experiment; - -, MNLS.

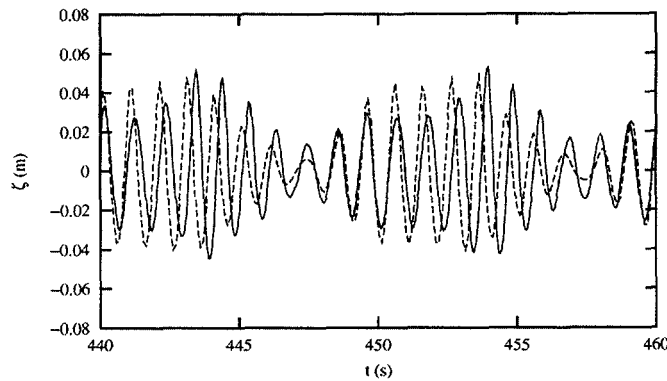


Figure 16: Test 61, staff 4 at 80 m,  $\eta = 5.7$ : —, experiment; - -, MNLS.